

Machine learning interatomic potential for high-throughput screening and optimization of high-entropy alloys

Anup Pandey^{1*}, Jonathan Gigax² and Reeju Pokharel¹

¹Material Science and Technology, Los Alamos National Laboratory, Los Alamos, NM 87545, USA.

²Center for Integrated Nanotechnologies, Los Alamos National Laboratory, Los Alamos, NM 87545, USA.

*Corresponding author(s). E-mail(s): anup@lanl.gov;
Contributing authors: jgigax@lanl.gov; reeju@lanl.gov;

Abstract

We have developed a machine learning-based interatomic potential (MLIP) for the quaternary MoNbTaW (R4) and quinary MoNbTaTiW (R5) high-entropy alloys (HEAs). MLIPs enabled accurate high-throughput calculations of elastic and mechanical properties of various non-equimolar R4 and R5 alloys, which are otherwise very time-consuming calculations when performed using density functional theory (DFT). We demonstrate that the MLIP predicted properties compare well with the DFT results on various test cases and are consistent with the available experimental data. The MLIPs are also utilized for high-throughput optimization of non-equimolar R4 candidates by guided iterative tuning of R4 compositions to discover candidate materials with promising hardness-ductility combinations. We also used this approach to study the effect of Ti concentration on the elastic and mechanical properties of R4, by statistically averaging the properties of over 100 random structures. MLIP predicted hardness and bulk modulus of equimolar R4 and R5 HEAs are validated using experimentally measured Vicker's hardness and modulus. This approach opens a new avenue for employing MLIPs for HEA candidate optimization.

Keywords: Machine Learning Interatomic Potential (MLIP), Moment Tensor Potential (MTP), High-entropy alloys (HEAs), Density functional theory (DFT)

1 Introduction

Alloy development is a costly, multi-year exercise. Selection of elements that produce a material with desired properties requires careful consideration of multi-component interactions. Further compounding on this difficulty is the perpetual need to optimize existing alloys for different applications, such as those for high temperature or radiation environments. The development of a computationally-based methods would serve to significantly reduce the exploratory cost when designing a new alloy or optimizing existing alloys.

Highly accurate first principles calculations are limited by the simulated length and time scale. Therefore, it is practically impossible to explore the vast configurational space of multi-component alloys (MCAs) using computationally demanding *ab initio* methods such as density functional theory (DFT). On the other hand, molecular dynamics (MD) simulations based on empirical force fields are much faster but limited to a few candidates of multi-component alloys (MCAs) due to the lack of accurate potentials. Therefore, machine learning potentials or force fields trained from the relatively small data sets obtained from the highly accurate quantum mechanical calculations can be a suitable alternative, with an accuracy of *ab initio* methods and efficiency over order of magnitudes than the DFT. Besides, the MLIPs, once trained, interpolate over a wide range of material compositions without requiring repeated DFT calculations for all of them, which enables high-throughput search of novel MCAs with desired properties.

Because of their computational efficiency and accuracy, MLIPs have recently gained wide attention in various branches of science [1–5]. Most machine learning potentials (MLPs) comprise of two parts: 1) the functional form called the "descriptors", which describes the local chemical environment satisfying the rotations, translations, and reflections symmetries, as well as the permutation of chemically equivalent elements. 2) A regressor, which maps the local environment to the potential energy and its derivative. In 2007, Behler and Parrinello introduced an artificial neural network (NN) as a regressor for MLIP development, which has recently been adopted in various studies [6–9]. Bartok *et al.* used Gaussian process regression to build their MLIP, which is called Gaussian Approximate Potentials (GAP) [10]. Alternatively, spectral neighbor analysis potential (SNAP) and moment tensor potential (MTP) are based on linear regression with a set of basis functions [11–13].

In this work, we have used the MTP-based approach, as implemented in the MLIP package [13]. The MTPs models are successfully trained for quaternary MoNbTaW (R4) and quinary MoNbTaTiW (R5) refractory high-entropy alloys (HEAs). Unlike conventional alloys, refractory HEAs have high melting point and high strength at elevated temperatures, which make them a suitable candidates for the structural applications [14, 15]. However, refractory HEAs are brittle at room temperature, which limits their broader applicability [16]. On the other hand, HEAs can have a non-equimolar combination of principle elements and do not restrict the addition of minor elements [14, 17], allowing for a myriad of unexplored alloys with prominent properties. There have

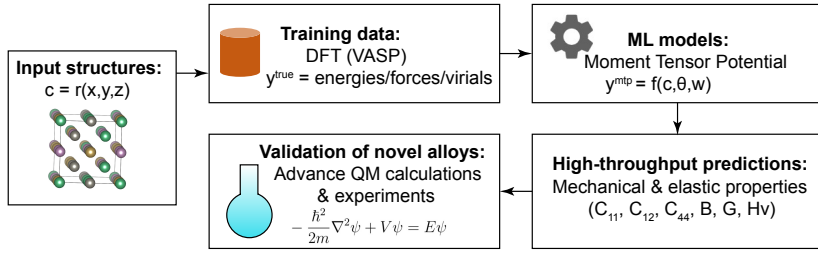


Fig. 1: Schematic representation of the workflow for training the MTP interatomic potential for performing high-throughput screening of high-entropy alloys for superior mechanical and elastic properties.

been some studies that show better properties of non-equimolar compositions compared to their equimolar counterparts [18, 19].

The use of MLIP in optimizing the HEA properties is nominal. Most of the machine learning based predictive models for alloys are based on data available in literature or DFT calculated properties [20–22]. Such data sets are very small and are unlikely to accurately predict a wide range of properties for the vast configuration space of these alloys. Only recently, MLIPs have been used for efficient optimization of HEA properties [23–25]. In this work, we demonstrate the application of MLIPs for high-throughput screening of novel HEAs that exhibit promising hardness-ductility combinations, which addresses the hardness-ductility trade-off in HEAs [19, 26]. This screening is carried out in for cases: (1) the non-equimolar compositions of R4 and (2) the Ti alloying in R4 (or R5). The MLPs are used for statistical averaging over numerous equimolar and non-equimolar configurations to adequately describe the systems for which DFT calculations alone would be extremely time-consuming and computationally intractable.

The training data sets are generated from the DFT calculations, which are described in the method section below. The trained models or MLIPs are incorporated in the well-known MD package LAMMPS for high-throughput elastic and mechanical properties calculations.

2 Methods

2.1 Computational methods

Moment tensor potential (MTP) describes the atomic contribution of an atom i to the total energy as:

$$V_{atom}^{MTP}(\mathbf{r}_i) = \sum_{j=1}^m \theta_j B_j(\mathbf{r}_i) \quad (1)$$

where B_j are the pre-defined basis functions, m is the number of functions in the basis, and θ are the fitting parameters. The total energy of a configuration

is given by:

$$E_{Total}^{MTP}(c) = \sum_{i=1}^{N_{atm}} V_{atom}^{MTP}(\mathbf{r}_i) \quad (2)$$

where N_{atm} is the total number of atoms in a configuration c . The functional form of the basis function B_j is defined by the moment tensor descriptors:

$$M_{\alpha,\beta}(\mathbf{r}) = \sum_j f_{\alpha}(|\mathbf{r}_{ij}|, z_i, z_j) \mathbf{r}_{ij}^1 \otimes \cdots \otimes \mathbf{r}_{ij}^{\beta} \quad (3)$$

where f_{α} is the radial part and $\mathbf{r}_{ij}^1 \otimes \cdots \otimes \mathbf{r}_{ij}^{\beta}$ is the angular part of the moments. The functional form and other details of the moments are discussed in [12, 13]. Then, the force acting on the j^{th} atom is given by:

$$f_j^{MTP}(c) = -\nabla_{x_j} E_{Total}^{MTP}(c) \quad (4)$$

where x_j is the atomic position. Similarly, the virial, the volume weighted stress components are given by,

$$\sigma^{MTP}(c) = \frac{1}{\det(\mathbf{a})} (\nabla_a E_{Total}^{MTP}(c)) \mathbf{a}^T \quad (5)$$

where \mathbf{a} is the lattice vector. Then, the value of θ_j are determined by minimization of the cost functional (L) given by:

$$L = \sum_{c \in C_{all}} [w_E^2 \Delta E(c)^2 + w_f^2 \sum_{j=1}^{N_{atm}} \Delta f_j(c)^2 + w_{\sigma}^2 \Delta \sigma(c)^2] \quad (6)$$

where, C_{all} is total configurations, $\Delta E = E^{MTP} - E^{DFT}$ is the error in total energy. Similarly, Δf and $\Delta \sigma$ are the errors in forces and virials, respectively. w_E , w_f , and w_{σ} are the weight factors for total energy, force, and stress, respectively. We have implemented the workflow illustrated in Fig.1 for training the MPT interatomic potential.

The training and validation data sets to fit the MTP potentials are obtained from the quantum mechanical calculations within the density functional theory (DFT) framework. DFT calculations were performed using the VASP package [27]. The electron-ion interactions are described by a projector augmented wave (PAW) [28], and the generalized gradient approximation of Perdew-Burke-Ernzerhof is used as an exchange-correlation function [29]. The DFT calculations for quaternary MoNbTaW (R4) are carried out using a 32-atom $2 \times 2 \times 4$ bcc supercell with randomized atoms. For quinary MoNbTaTiW (R5), a 40-atom $2 \times 2 \times 5$ bcc supercell with a randomized atom is used as a starting structure. The data are generated in two ways: 1) from *ab initio* molecular dynamics (AIMD) sampling for 20000 steps (20 ps) at a time step of 1fs, 2) from the single point (SP) energy, forces, and virial calculations for random alloys. For AIMD, 400 eV cut-off energy and the k-mesh of $2 \times 2 \times 1$ are taken for both

R4 and R5. The configurations after every 50 steps are subjected to SP calculations with stringent cut-off energy of 500 eV and k-mesh of $6 \times 6 \times 3$ for both R4 and R5. For the SP calculation of random alloys, the cut-off energy of 500 eV and k-mesh of $6 \times 6 \times 3$ is taken for all the cases. The AIMD simulations are carried out at temperatures 500K, 1000K, and 1500K with a 2% increase and decrease in the lattice parameters for each temperature. The random alloys for SP calculations comprise alloys sampled with random compositions, volume (2% increase and decrease in volume), and shape (2% increase and decrease in lattice angle). While training the MTP model, 800 configurations were randomly chosen from AIMD and SP generated configurations. The static and elastic properties are calculated in LAMMPS [30] with the trained interatomic potentials.

For bcc cubic phase, there are three independent single-crystal elastic constants: C_{11} , C_{12} , and C_{44} . For the supercell model we adopted, there are nine independent elastic constants due to low symmetry and large cell size [31]. Therefore, we took the average of the calculated elastic constant as follows:

$$\begin{aligned} C_{11} &= \frac{C'_{11} + C'_{22} + C'_{33}}{3} \\ C_{12} &= \frac{C'_{12} + C'_{23} + C'_{13}}{3} \\ C_{44} &= \frac{C'_{44} + C'_{55} + C'_{66}}{3} \end{aligned} \quad (7)$$

where the elastic constants on the right-hand side are the ones obtained from calculations. The elastic constants are calculated from the optimized structures from the stress-strain relationship method as implemented in the VASP and LAMMPS. The Voigt-Reuss-Hill (VRH) approximation [32] is used to calculate the bulk modulus (B) and shear modulus (G) of the polycrystalline materials from the elastic constants C_{ij} of a single crystal. B and G in VRH approximation is given by [33, 34]:

$$\begin{aligned} B_{VRH} &= \frac{B_V + B_R}{2}, \\ G_{VRH} &= \frac{G_V + G_R}{2} \end{aligned} \quad (8)$$

where B_V and G_V is Voigt's bulk modulus and shear modulus, and B_R and G_R are Reuss's bulk modulus and shear modulus, respectively. For cubic phase,

they are given by:

$$\begin{aligned} B_V &= B_R = \frac{C_{11} + 2C_{12}}{3}, \\ G_V &= \frac{C_{11} - C_{12} + 3C_{44}}{5}, \\ G_R &= \frac{5(C_{11} - C_{12})C_{44}}{4C_{44} + 3(C_{11} - C_{12})}. \end{aligned} \quad (9)$$

The mechanical stability criteria as suggested by Born and Huang are given by [35]:

$$C_{11} > 0, C_{44} > 0, C_{11} > C_{12}, (C_{11} + 2C_{12}) > 0 \quad (10)$$

The ductility of materials is estimated through Pugh's criterion: the condition for the ductility of materials is that the Pugh's ratio (B/G) should be greater than 1.75 [36]. Also, the Cauchy pressure ($C_{11}-C_{44}$) is positive in a ductile material and negative in the brittle material [37]. The microhardness is calculated using the Cheng *et al.* model for Vicker's hardness which is based on Pugh modulus ratio $k=B/G$ and is given by [38]:

$$H_V = 2(k^2 G)^{0.585} - 3 \quad (11)$$

Table 1: Parameters for MTP model.

Parameter	Value (MoNbTaW)	Value (MoNbTaTiW)
Radial functions	4	5
Radial basis size	8	8
alpha moments count	350	1352
alpha index basic count	130	295
alpha index times count	969	6349
alpha scalar moments	92	288
Cutoff	5.0 Å	5.0 Å
Stress weight	1×10^{-3}	1×10^{-3}
Force weight	1×10^{-2}	1×10^{-2}
Energy weight	1	1
BFGS iterations	1000	1000

2.2 Experimental methods

The R4 and R5 alloys were purchased from Sophisticated Alloys. All specimens were ground to a 4000 grit SiC paper and further polished to a final solution of 0.04 μm silica. A Thermo-Fisher G4 plasma focused ion beam/scanning

Table 2: Bulk properties of 2X2X4 supercell (32-atom) of equimolar MoNbTaW and 2X2X5 supercell (40-atom) supercell of MoNbTaTiW obtained from the SQS. The properties are calculated using DFT and MPT at 0K.

	MoNbTaW (SQS)		MoNbTaTiW (SQS)	
	DFT	MTP	DFT	MTP
C11 (GPa)	371.29	356.70 (3.9%)	297.27	288.17 (3.06%)
C12 (GPa)	159.93	165.72 (-3.6%)	149.49	158.15 (-5.8%)
C44 (GPa)	75.36	68.00 (9.8%)	54.99	42.43 (22.8%)
VRH Bulk Modulus (B) (GPa)	230.38	229.38 (0.43%)	198.75	201.49 (-1.4%)
VRH Shear Modulus (G) (GPa)	86.31	77.92 (9.72%)	61.91	50.37 (18.63%)
Cauchy Pressure (C11-C44) (GPa)	84.57	97.72	94.49	115.72
Vicker's Hardness (GPa)	5.60	4.23	2.71	0.91
Pugh's Criterion (B/G)	2.67	2.94	3.21	4.00

electron microscope was used to produce elemental maps of the HEAs. Nanoindentation tests, used to measure the hardness and modulus of the HEAs, were performed on a Keysight G200 Nanoindenter equipped with a diamond Vicker's tip. All indents were made to a final displacement of 2,000 nm with a constant strain rate (loading rate divided by the load) of 0.05 s^{-1} . Continuous stiffness measurements (CSM) were performed at a frequency of 45 Hz and 2 nm displacement amplitude. Hardness and modulus measurements were determined using the Oliver-Pharr method [39]. The tip area function was calibrated by indenting fused silica and using tip properties with a Young's modulus and Poisson's ratio of 1130 GPa and 0.07 (diamond).

Table 3: Bulk properties of equimolar MoNbTaW at 0K obtained from MTP by averaging over 50 randomly ordered 432-atom system alloys. The results are compared with the DFT results averaged over 5 random alloys.

	a (Å)	B (GPa)	C11 (GPa)	C12 (GPa)	C44 (GPa)
MTP	3.241 ± 0.0010	231.12 ± 0.51	355.39 ± 1.01	168.97 ± 0.42	69.60 ± 0.37
DFT	3.241 ± 0.0002	231.44 ± 0.3	375.15 ± 0.85	159.58 ± 0.76	74.98 ± 3.23

3 Results and Discussion

The optimized parameters for the trained MTP models for the two different alloy systems are shown in Table 1.

3.1 MTP for quaternary MoNbTaW

The training history for quaternary MoNbTaW (R4) is shown in Fig.2, Fig.3, and Fig.4. It can be seen that the MTP predicted energy, force, and virial

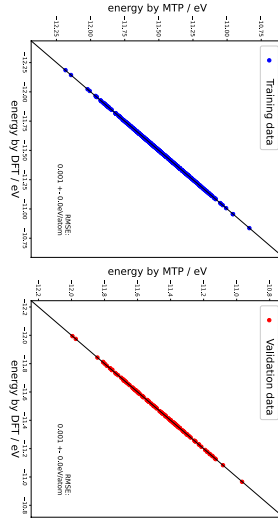


Fig. 2: Comparison of total energy of quaternary MoNbTaW alloys with different compositions from DFT and MTP predictions, shown for training (left) and validation (right) data sets.

compare well with the DFT calculated values (ground truth). The accuracy for MTP is within 0.041 eV for energies, 0.021 eV/Å for forces, and 0.383 eV for virials for the validation data. This verifies that the potential is accurate for any given composition of MoNbTaW. The equation of state at 0K for an equimolar R4 obtained from MTP is compared to the DFTs in Fig.5(a). The energy-volume (EV) curve compares well with the DFT, suggesting that the ML-based potential can describe the elastic response accurately. The bulk modulus obtained by fitting the EV data from DFT to the Birch-Murnaghan equation of state [40] is 229.39 GPa. We have adopted a special quasi-random supercell (SQS) [41] (implemented in the icet package https://icet.materialsmodeling.org/advanced_topics/sqs_generation.html) method to generate a $2 \times 2 \times 4$ supercell (32-atom) of equimolar R4. The MTP MLIP is further validated by calculating the elastic constants and related properties for the SQS model by incorporating the MTP in the LAMMPS package and comparing with the corresponding results from the DFT as shown in Table 2. The elastic moduli predicted by MTP are in excellent agreement with the DFT with errors $< 5\%$ except for a slight overestimation of C_{44} (% error 9.8%) and corresponding shear modulus (% error 9.72%). The predictions are better compared to the one from the SNAP machine learning model, where the percentage errors on C_{11} , C_{12} , C_{44} , B, and G are 5.8%, 3.8%, 15.9%, 4.3% and 13.3%, respectively [42]. The Vicker's hardness for the SQS model from

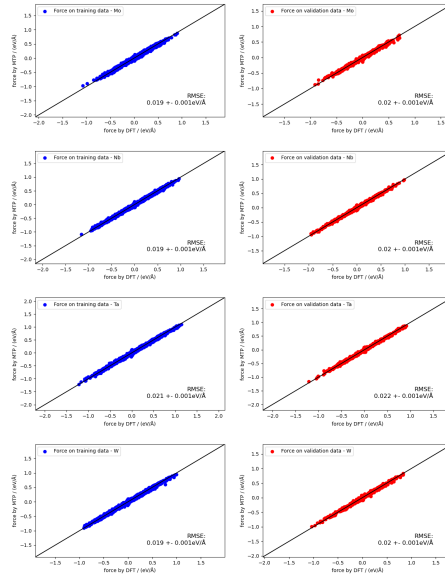


Fig. 3: Comparison of forces on quaternary MoNbTaW (both equimolar and non-equimolar compositions) from DFT calculations (ground truth) and MTP predictions on each element for the training (left) and validation (right) data sets.

the DFT and MTP model are 5.60 GPa and 4.23 GPa, respectively. These values are in a good agreement with the experimental value 4.455 GPa [16]. The strained SQS models are not included in the training data, yet the MTP model is robust enough to perform well for the R4 SQS model, which is the strong validation of generalization of the MTP model.

We have experimentally measured nanoindentation Vicker's hardness and modulus for MoNbTaW, which are 8.06 ± 0.31 GPa and 214.4 ± 2.6 GPa, respectively. Usually, the nanoindentation measurements are overestimated compared to other indentation techniques [43]. The nanoindentation bulk modulus compares really well with the DFT calculated value of 230.38 GPa (6.9 % error).

In order to ensure the statistical reproducibility, we have computed average bulk properties of equimolar MoNbTaW from 50 random 432-atom systems using the MTP, which is shown in Table 3. Such type of statistical sampling is not easily achievable by the DFT. The results from MTP are compared with the DFT results averaged over 5 random 32-atom systems. The lattice

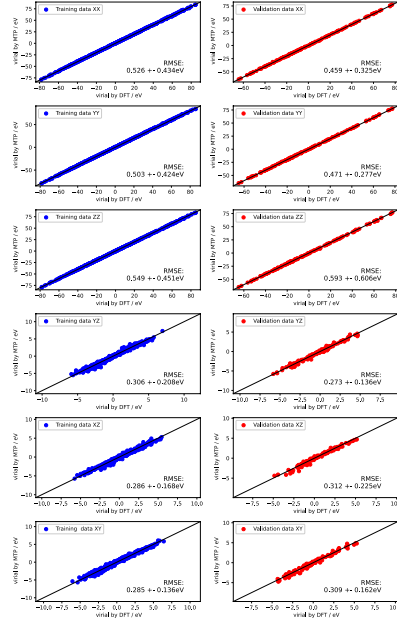


Fig. 4: Comparison of six virial components on quaternary MoNbTaW (both equimolar and non-equimolar compositions) from DFT calculations (ground truth) and MTP predictions for training (left) and validation (right) data sets.

constant calculated from both the MTP and DFT are 3.241\AA , which is close to the experimental value 3.213\AA [16] and the theoretical value 3.271\AA [44].

3.2 Rational design of non-equimolar MoNbTaW

The configurational space for non-equimolar MoNbTaW spans over several orders of magnitudes. It is computationally impossible to screen the components for optimal properties using the highly expensive DFT calculations, before carrying out the expensive experiment. As a test case, we have tweaked the compositions of adjacent atomic number elements pair, Mo-Nb pair and Ta-W pair, one at a time by 12.5%, 25%, 37.5%, and 50% and screened their elastic response using the MTP. Also, we tested four cases of mixed variations in all four components by 25% and 50%. The MTP predicted total energies for twenty non-equimolar structures are in excellent agreement with the

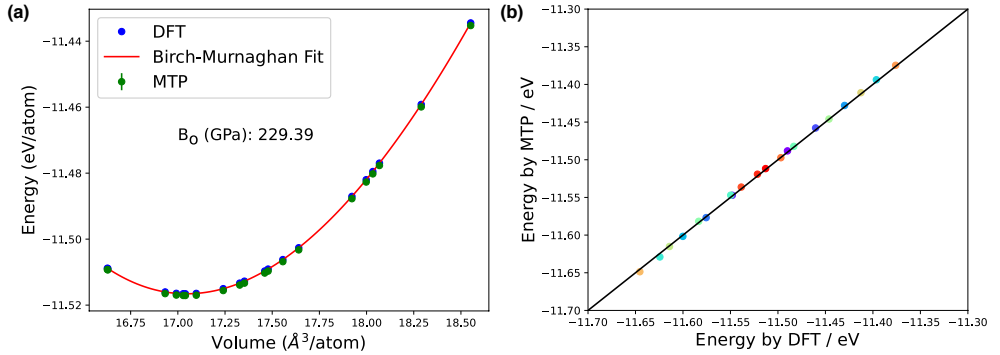


Fig. 5: (a) Comparison of energy per atom as a function of volume for an equimolar MoNbTaW random alloy obtained from MTP and DFT. Solid red line is the Birch-Murnaghan fit to the DFT data. (b) Comparison of energy per atom for 20 random 64-atom non-equimolar MoNbTaTiW obtained from MTP and DFT. Colors correspond to different structures.

DFT, as shown in Fig.5 (b). The bulk and shear modulus of the twenty non-equimolar structures are shown in Fig.6(a) and Fig.6(b). The Pugh's criterion and Vicker's hardness are shown in Fig.6 (c) and Fig.6 (d).

It can be seen that reducing the Mo composition and increasing the Nb composition lowers the hardness and improves the ductility ($\text{Mo}_{0.875}\text{Nb}_{1.125}\text{TaW}$, $\text{Mo}_{0.75}\text{Nb}_{1.25}\text{TaW}$, $\text{Mo}_{0.625}\text{Nb}_{1.375}\text{TaW}$, and $\text{Mo}_{0.5}\text{Nb}_{1.5}\text{TaW}$). On the other hand, increasing the Mo compositions and decreasing the Nb composition increases the hardness and decreases the ductility ($\text{Mo}_{1.125}\text{Nb}_{0.875}\text{TaW}$, $\text{Mo}_{1.25}\text{Nb}_{0.75}\text{TaW}$, $\text{Mo}_{1.375}\text{Nb}_{0.625}\text{TaW}$, and $\text{Mo}_{1.5}\text{Nb}_{0.5}\text{TaW}$). Similarly, increasing Ta compositions and reducing W decreases the hardness and improves the ductility ($\text{MoNbTa}_{1.125}\text{W}_{0.875}$, $\text{MoNbTa}_{1.25}\text{W}_{0.75}$, $\text{MoNbTa}_{1.375}\text{W}_{0.625}$, and $\text{MoNbTa}_{1.5}\text{W}_{0.5}$). However, reducing the Ta compositions and increasing the W compositions improves the hardness and reduces the ductility ($\text{MoNbTa}_{0.875}\text{W}_{1.125}$, $\text{MoNbTa}_{0.75}\text{W}_{1.25}$, $\text{MoNbTa}_{0.625}\text{W}_{1.375}$, and $\text{MoNbTa}_{0.5}\text{W}_{1.5}$). There is no significant variation in the hardness and ductility when all four compositions are varied in a mixed way ($\text{Mo}_{1.5}\text{Nb}_{0.5}\text{Ta}_{1.5}\text{W}_{0.5}$, $\text{Mo}_{0.5}\text{Nb}_{1.5}\text{Ta}_{0.5}\text{W}_{1.5}$, $\text{Mo}_{0.875}\text{Nb}_{1.125}\text{Ta}_{0.875}\text{W}_{1.125}$, and $\text{Mo}_{1.125}\text{Nb}_{0.875}\text{Ta}_{1.125}\text{W}_{0.875}$).

Some non-equimolar R4 candidates with promising hardness-ductility combinations, for example $\text{Mo}_{0.75}\text{Nb}_{1.25}\text{TaW}$ ($B/G = 3.04$, $H_V = 3.72$), $\text{Mo}_{0.625}\text{Nb}_{1.375}\text{TaW}$ ($B/G = 3.07$, $H_V = 3.53$), $\text{MoNbTa}_{1.25}\text{W}_{0.75}$ ($B/G = 3.02$, $H_V = 3.79$), and $\text{MoNbTa}_{1.375}\text{W}_{0.625}$ ($B/G = 3.08$, $H_V = 3.50$), than the equimolar R4 ($B/G = 2.94$, $H_V = 4.23$) are predicted by the MTP. The predicted alloy candidates can be experimentally designed and characterized [45–48] for further validation.

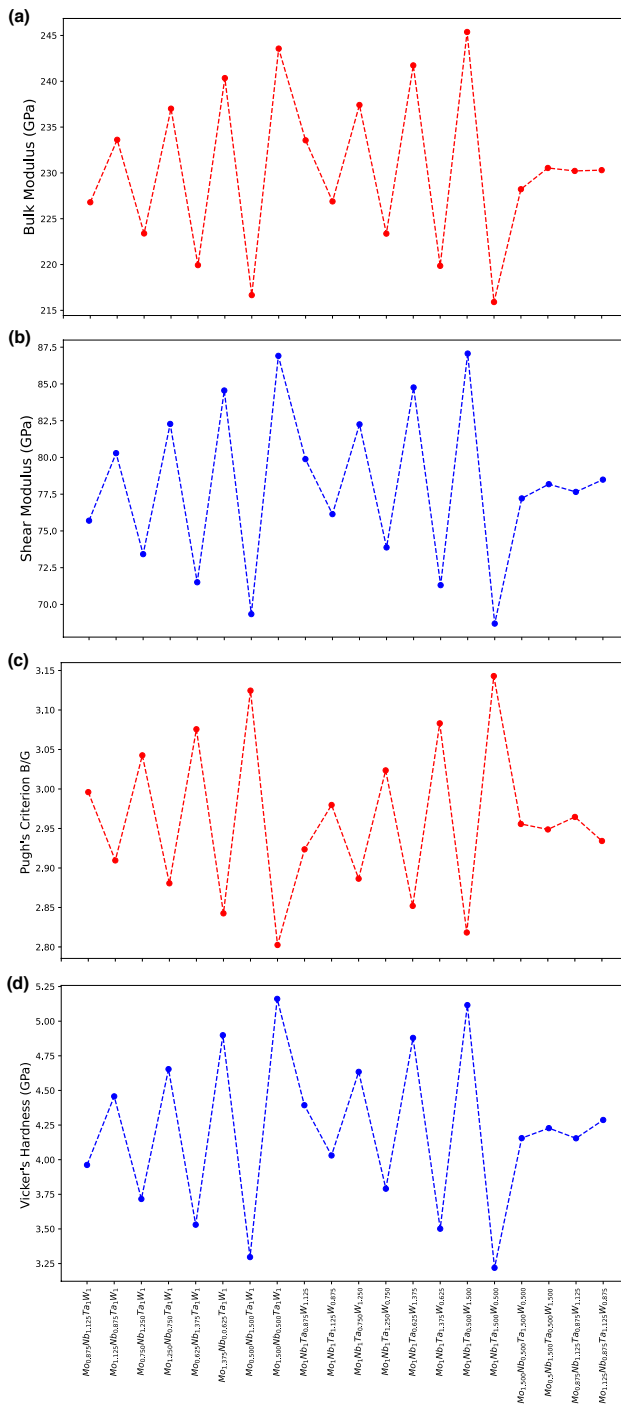


Fig. 6: (a) Bulk modulus (b) shear modulus (c) Pugh's Criterion, and (d) Vicker's Hardness for the twenty random 64-atom non-equimolar MoNbTaTiW obtained from MTP.

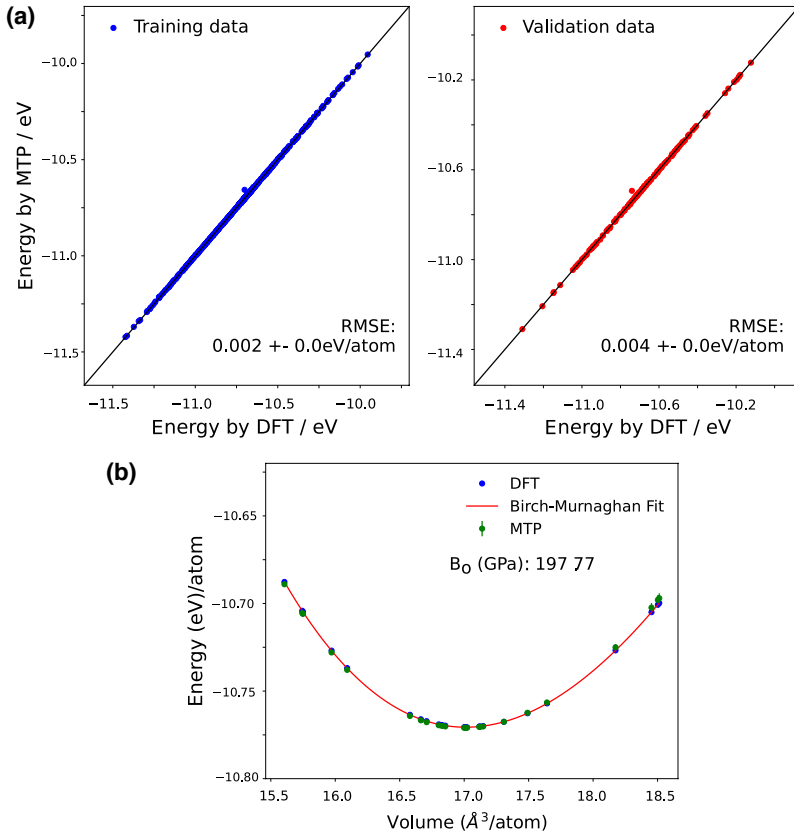


Fig. 7: (a) Comparison of total energy of quinary MoNbTaTiW alloys with different compositions from DFT and MTP predictions, shown for training (left) and validation (right) data sets. (b) Comparison of energy per atom as a function of volume for an equimolar MoNbTaTiW random alloy obtained from MTP and DFT. Solid red line is the Birch-Murnaghan fit to the DFT data.

3.3 Alloying effect of Ti on MoNbTaW

Although it is well established that the mechanical properties can be significantly improved by alloying, experimentally it is not feasible to fabricate and test the alloys with multiple possible compositions in a systematic way. Therefore, it is imperative to have a tool that can provide a high-throughput screening of the various fraction of the alloying element for a desired property and can guide the experiments. This section will demonstrate the applicability of MLIP in the high-throughput investigation of alloying effect of Ti in the elastic and mechanical properties of R4.

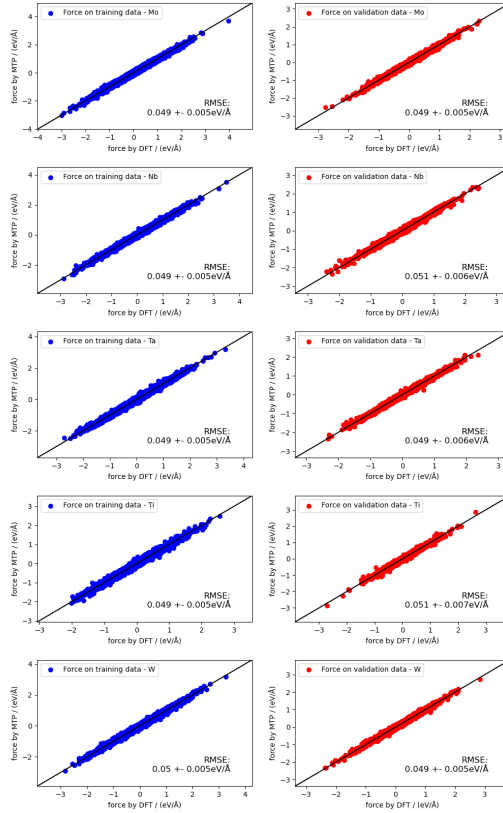


Fig. 8: Comparison of forces on quinary MoNbTaTiW (both equimolar and non-equimolar compositions) from DFT calculations (ground truth) and MTP predictions on each component for training (left) and validation (right) data sets.

3.3.1 MTP for quinary MoNbTaTiW

We have trained a separate MTP with the training data described in the computational method section above. The training parameters are shown in Table 1. The training history for quinary MoNbTaTiW (R5) is shown in Fig.7(a), Fig.8, and Fig.9. The predicted energy, force, and virial compare well with the DFT results (ground truth). The accuracy of MTP is within 0.151 eV

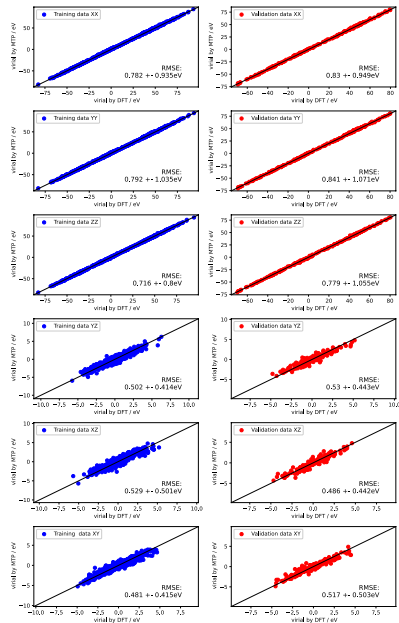


Fig. 9: Comparison of six virial components on quinary MoNbTaTiW (both equimolar and non-equimolar compositions) from DFT calculations (ground truth) and MTP predictions for training (left) and validation (right) data sets.

for energies, 0.050 eV/Å for forces, and 0.630 eV for virials for the validation data, which verifies that the potential is accurate for any given composition of MoNbTaW. As in the case of R4, the equation of state at 0K for an equimolar R5 obtained from MTP compares well with the DFTs as shown in Fig.7(b), suggesting that the ML potential can describe the elastic response accurately. The bulk modulus obtained by fitting the energy-volume data of the DFT to the Birch-Murnaghan equation of state [40] is 197.77 GPa. As in R4, a $2 \times 2 \times 5$ supercell (40-atom) SQS model of equimolar R5 is generated. The MTP potential is further validated by calculating the elastic constants and bulk properties for the SQS model and comparing with the corresponding DFT results as shown in Table 2. The elastic moduli predicted by MTP are in excellent agreement with the DFT with errors <5%, except for a slight overestimate for the C_{44} (% error 22.8%) and corresponding shear modulus (% error 18.63%). Again, the strained SQS models are not included in the training data, yet the MTP model is robust enough to perform well for SQS

Table 4: Bulk properties prediction for random MoNbTaTi_{0.5}W. The properties are calculated using DFT and MTP at 0K. The values from DFT are averages over 5 random structures and that from MTP are averaged over 100 random 180-atom structures

	MoNbTaTi _{0.5} W	
	DFT	MTP
C11 (GPa)	319.91±5.92	323.14±1.61 (-1.01%)
C12 (GPa)	158.15±2.16	159.18±0.43 (-0.65%)
C44 (GPa)	55.44±6.84	44.20±0.49 (20.27%)
VRH Bulk Modulus (B) (GPa)	212.07	213.83 (-0.83%)
VRH Shear Modulus (G) (GPa)	64.47	56.75 (11.97%)
C11-C44 (GPa)	264.47	114.99
Vicker's Hardness (Hv)	2.68	1.50
Pugh's Criterion (B/G)	3.29	3.78

R5, which is the strong validation of generalization of the MTP model. The Vicker's hardness for the SQS model from the DFT and MTP model are 2.71 GPa and 0.91 GPa, respectively. The difference in the Vickers's hardness is due to the error in the predicted shear modulus.

We have experimentally measured nanoindentation Vicker's hardness and bulk modulus for MoNbTaTiW, which are 7.58 ± 0.30 GPa and 197.3 ± 7.20 GPa, respectively. The experimentally measured bulk modulus, shear modulus, and the Vicker's hardness of R5 as reported by Han *et al.* are 139 GPa, 59 GPa, and 4.89 GPa, respectively [15]. The nanoindentation bulk modulus compares really well with the DFT calculated value of 198.75 GPa (0.73 % error).

In this work, the DFT calculated bulk modulus and shear modulus for the SQS model is 198.75 GPa and 61.91 GPa, respectively. Mishra *et al.* calculated the bulk modulus and shear modulus for the R5 using supercell models and the DFT, which are reported as 193.90 GPa and 70.67 GPa, respectively [49]. Similarly, Bhandari *et al.* calculated B and G using the Knuth-shuffle supercell model and the DFT, which are 199 GPa and 60 GPa, respectively [50]. This shows that the theoretical results for various models are pretty consistent. There is a considerable discrepancy in the theoretically reported Vicker's hardness and the experimentally measured ones [15], which calls for the further experimental investigations.

3.3.2 Statistical study of alloying effect

We have computed the average bulk properties of MoNbTaTi_{0.5}W from 100 random 180-atom systems using the MTP, which is shown in Table 4. The results are compared with the DFT calculated values averaged over 5 random 36-atom systems. The elastic moduli predicted by the MTP are in excellent agreement with the DFT with errors around 1%, except for the C₄₄ (% error 20.27%) and corresponding shear modulus (% error 11.97%). The % error for C₄₄ (and the corresponding shear modulus) for MoNbTaTiW and the

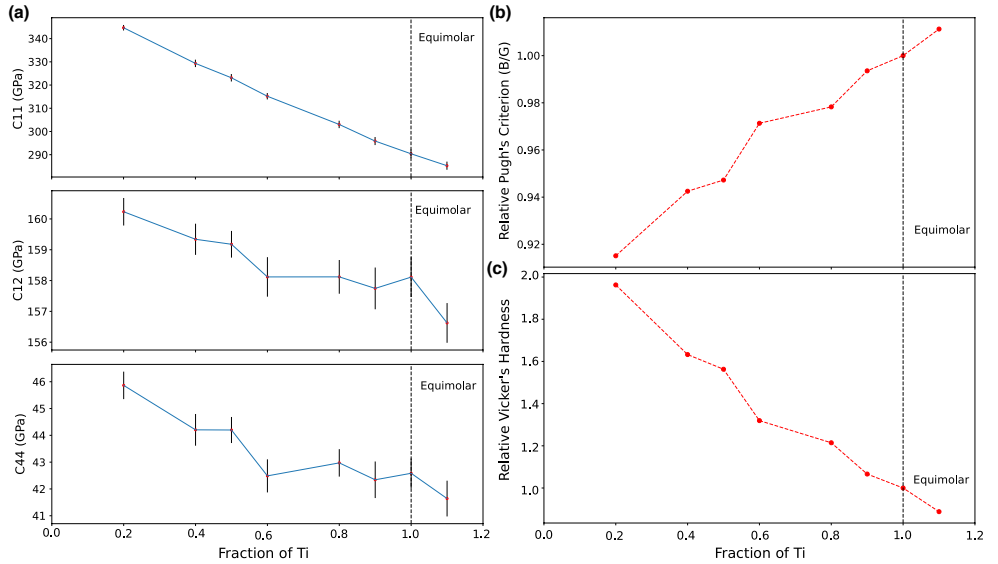


Fig. 10: (a) Components of elastic constants for MoNbTaTi_xW ($x=0.2, 0.4, 0.5, 0.6, 0.8, 1.0$, and 1.1), obtained from MTP by averaging over 100 random structures for each composition. Error bars indicate the the standard deviations for 100 structures at each composition. (b) Pugh's criterion (B/G)) relative to the equimolar MoNbTaTiW, and (c) Vicker's hardness relative to the equimolar MoNbTaTiW obtained from MTP for the nine different Ti concentrations.

MoNbTaTi_{0.5}W are consistent, suggesting that the MTP predictions for C_{44} are standardized and can be used in a comparative investigation of other Ti compositions. It should be noted that since the random structures are included in the training sets, the predictions are better than the SQS model.

The elastic constants predicted for MoNbTaTi_xW ($x=0.2, 0.4, 0.5, 0.6, 0.8, 1.0$, and 1.1) are shown in Fig.10 (a), where the error bars are the standard deviations for 100 random structures. The Pugh's ratio and the Vicker's hardness predicted for 9 different Ti concentrations relative to the equimolar R5 are shown in Fig.10(b) and Fig.10(c), respectively. The MTP model captures the inverse behavior of ductility (B/G) and the hardness with the addition of the Ti. The addition of Ti reduces the hardness and improves the ductility, which corroborates with the experimental results [15]. As shown in Fig.10, the alloys, for example, MoNbTaTi_{0.5}W and MoNbTaTi_{0.8}W, with Ti composition other than the widely investigated equimolar MoNbTaTiW have promising hardness-ductility combination, which requires further experimental investigations.

We have demonstrated that MTP-MLIP successfully reproduces the *ab initio* potentials of complex high-entropy alloys, at orders of magnitude lower

computational cost. The computational efficiency of MTP enabled the screening of vast configurational space occupied by R4 and R5 alloys to optimize their compositions by statistically averaging over hundreds of structures; otherwise not feasible using DFT calculations. Selective tuning of elemental compositions of R4 (Mo, Nb, Ta, W) enabled the discovery of novel refractory HEAs with promising hardness-ductility combinations. This approach was also successfully demonstrated for Ti alloying in R4. Hence, this method can be readily extended for high-throughput screening of other HEA systems and advanced theoretical study of novel alloys for accelerated materials discovery and design. Future work entails quantum mechanical calculations under desired thermo-mechanical conditions and corresponding experimental validation of promising alloy candidates (e.g., $\text{Mo}_{0.75}\text{Nb}_{1.25}\text{TaW}$ and $\text{MoNbTaTi}_{0.5}\text{W}$).

MTP-MLIP also exhibited improved accuracy compared to SNAP-MLIP [42] for the MoNbTaW HEA system studied in this work. Therefore, MTP-MLIP can be used to investigate advanced material phenomena at higher time scales such as the interplay between short-range order, segregation, strengthening, etc., through atomistic simulations, similar to that reported by Li *et al.* using the SNAP-MLIP method [42]. Computational efficiency and the accuracy of DFT also make MTP-MLIP a promising alternative to other ML models trained using material properties data obtained from limited published literature [20, 21].

There is a considerable discrepancy between the experimentally measured elastic and bulk properties of MoNbTaTiW by Han *et al.* and the DFT calculated ones. Therefore, for further validation, we have measured the Vicker's hardness and bulk modulus of MoNbTaW and MoNbTaTiW from the nanoindentation technique. The MTP predicted bulk modulus for both the alloys are in excellent agreement with our experimental bulk modulus. However, some inconsistencies exist between the experimentally measured and theoretically calculated Vicker's hardness [15].

4 Conclusion

We have successfully trained MTP machine learning potentials for quaternary MoNbTaW and quinary MoNbTaTiW HEAs. High-throughput calculations of elastic and mechanical properties of hundreds of novel structures are feasible with MTP-MLIP, which are highly time-consuming using DFT calculations. MTP-MLIPs enabled the rational design of non-equimolar alloys leading to the discovery of novel HEAs with enhanced hardness-ductility combinations (e.g., $\text{Mo}_{0.75}\text{Nb}_{1.25}\text{TaW}$). Computationally efficient and accurate MLIPs are reliable predictive tools for high-throughput optimization of alloying elements and screening of other high-entropy alloys. The approach presented here will significantly reduce the exploratory cost when designing a new alloy or optimizing existing ones.

5 Acknowledgements

This work was supported by the US Department of Energy through Los Alamos National Laboratory. Los Alamos National Laboratory (LANL) is operated by Triad National Security, LLC, for the National Nuclear Security Administration of the US Department of Energy (Contract No. 89233218CNA000001). This work was funded by Institute for Materials Science, Rapid Response Award and LANL’s Laboratory Directed Research and Development Project #20190571ECR. The experimental work was performed, in part, at the Center for Integrated Nanotechnologies, an Office of Science User Facility operated by LANL. The use of LANL’s HPC institutional computing for the computational time is also acknowledged. We would also like to thank Dr. Ghanshyam Pilania and Dr. Danny Perez for fruitful discussions.

6 Conflict of Interest

The authors declare no conflict of interest.

References

- [1] Unke, O.T., Chmiela, S., Sauceda, H.E., Gastegger, M., Poltavsky, I., Schütt, K.T., Tkatchenko, A., Müller, K.-R.: Machine learning force fields. *Chemical Reviews* (2021)
- [2] Musil, F., Grisafi, A., Bartók, A.P., Ortner, C., Csányi, G., Ceriotti, M.: Physics-inspired structural representations for molecules and materials. *Chemical Reviews* **121**(16), 9759–9815 (2021)
- [3] Deringer, V.L., Bartók, A.P., Bernstein, N., Wilkins, D.M., Ceriotti, M., Csányi, G.: Gaussian process regression for materials and molecules. *Chemical Reviews* **121**(16), 10073–10141 (2021)
- [4] Botu, V., Batra, R., Chapman, J., Ramprasad, R.: Machine learning force fields: construction, validation, and outlook. *The Journal of Physical Chemistry C* **121**(1), 511–522 (2017)
- [5] Ramprasad, R., Batra, R., Pilania, G., Mannodi-Kanakkithodi, A., Kim, C.: Machine learning in materials informatics: recent applications and prospects. *npj Computational Materials* **3**(1), 1–13 (2017)
- [6] Behler, J., Parrinello, M.: Generalized neural-network representation of high-dimensional potential-energy surfaces. *Phys. Rev. Lett.* **98**, 146401 (2007). <https://doi.org/10.1103/PhysRevLett.98.146401>
- [7] Behler, J.: Perspective: Machine learning potentials for atomistic simulations. *The Journal of chemical physics* **145**(17), 170901 (2016)

- [8] Smith, J.S., Isayev, O., Roitberg, A.E.: Ani-1: an extensible neural network potential with dft accuracy at force field computational cost. *Chemical science* **8**(4), 3192–3203 (2017)
- [9] Pun, G.P., Batra, R., Ramprasad, R., Mishin, Y.: Physically informed artificial neural networks for atomistic modeling of materials. *Nature communications* **10**(1), 1–10 (2019)
- [10] Bartók, A.P., Payne, M.C., Kondor, R., Csányi, G.: Gaussian approximation potentials: The accuracy of quantum mechanics, without the electrons. *Phys. Rev. Lett.* **104**, 136403 (2010). <https://doi.org/10.1103/PhysRevLett.104.136403>
- [11] Thompson, A.P., Swiler, L.P., Trott, C.R., Foiles, S.M., Tucker, G.J.: Spectral neighbor analysis method for automated generation of quantum-accurate interatomic potentials. *Journal of Computational Physics* **285**, 316–330 (2015)
- [12] Shapeev, A.V.: Moment tensor potentials: A class of systematically improvable interatomic potentials. *Multiscale Modeling & Simulation* **14**(3), 1153–1173 (2016)
- [13] Novikov, I.S., Gubaev, K., Podryabinkin, E.V., Shapeev, A.V.: The mlip package: moment tensor potentials with mpi and active learning. *Machine Learning: Science and Technology* **2**(2), 025002 (2020)
- [14] Miracle, D.B., Senkov, O.N.: A critical review of high entropy alloys and related concepts. *Acta Materialia* **122**, 448–511 (2017)
- [15] Han, Z., Chen, N., Zhao, S., Fan, L., Yang, G., Shao, Y., Yao, K.: Effect of ti additions on mechanical properties of nbmotaw and vnbmotaw refractory high entropy alloys. *Intermetallics* **84**, 153–157 (2017)
- [16] Senkov, O., Wilks, G., Miracle, D., Chuang, C., Liaw, P.: *Intermetallics*, 18. Iss **9**, 1758 (2010)
- [17] Gao, M.C., Yeh, J.-W., Liaw, P.K., Zhang, Y., et al.: *High-entropy alloys*. Cham: Springer International Publishing (2016)
- [18] Li, Z., Tasan, C.C., Pradeep, K.G., Raabe, D.: A trip-assisted dual-phase high-entropy alloy: grain size and phase fraction effects on deformation behavior. *Acta Materialia* **131**, 323–335 (2017)
- [19] Li, Z., Raabe, D.: Strong and ductile non-equiatomic high-entropy alloys: design, processing, microstructure, and mechanical properties. *Jom* **69**(11), 2099–2106 (2017)

- [20] Zhou, Z., Zhou, Y., He, Q., Ding, Z., Li, F., Yang, Y.: Machine learning guided appraisal and exploration of phase design for high entropy alloys. *npj Computational Materials* **5**(1), 1–9 (2019)
- [21] Chen, T.-C., Elveny, M., Surendar, A., Lawal, A.I., Zekiy, A.O., Anzum, R.: Developing a multilateral-based neural network model for engineering of high entropy amorphous alloys. *Modelling and Simulation in Materials Science and Engineering* **29**(6), 065019 (2021)
- [22] Bhandari, U., Zhang, C., Zeng, C., Guo, S., Adhikari, A., Yang, S.: Deep learning-based hardness prediction of novel refractory high-entropy alloys with experimental validation. *Crystals* **11**(1), 46 (2021)
- [23] Hart, G.L., Mueller, T., Toher, C., Curtarolo, S.: Machine learning for alloys. *Nature Reviews Materials* **6**(8), 730–755 (2021)
- [24] Grabowski, B., Ikeda, Y., Srinivasan, P., Körmann, F., Freysoldt, C., Duff, A.I., Shapeev, A., Neugebauer, J.: Ab initio vibrational free energies including anharmonicity for multicomponent alloys. *npj Computational Materials* **5**(1), 1–6 (2019)
- [25] Meshkov, E., Novoselov, I., Shapeev, A., Yanilkin, A.: Sublattice formation in cocrfeni high-entropy alloy. *Intermetallics* **112**, 106542 (2019)
- [26] Lei, Z., Liu, X., Wu, Y., Wang, H., Jiang, S., Wang, S., Hui, X., Wu, Y., Gault, B., Kontis, P., *et al.*: Enhanced strength and ductility in a high-entropy alloy via ordered oxygen complexes. *Nature* **563**(7732), 546–550 (2018)
- [27] Kresse, G., Furthmüller, J.: Efficient iterative schemes for ab initio total-energy calculations using a plane-wave basis set. *Physical review B* **54**(16), 11169 (1996)
- [28] Blöchl, P.E.: Projector augmented-wave method. *Physical review B* **50**(24), 17953 (1994)
- [29] Perdew, J.P., Burke, K., Ernzerhof, M.: Generalized gradient approximation made simple. *Physical review letters* **77**(18), 3865 (1996)
- [30] Plimpton, S.: Fast parallel algorithms for short-range molecular dynamics. *Journal of computational physics* **117**(1), 1–19 (1995)
- [31] Wen, Z., Zhao, Y., Tian, J., Wang, S., Guo, Q., Hou, H.: Computation of stability, elasticity and thermodynamics in equiatomic alcrfeni medium-entropy alloys. *Journal of Materials Science* **54**(3), 2566–2576 (2019)
- [32] Andrews, K.W.: Elastic moduli of polycrystalline cubic metals. *Journal*

- of Physics D: Applied Physics **11**(18), 2527–2534 (1978). <https://doi.org/10.1088/0022-3727/11/18/011>
- [33] Wu, Z.-j., Zhao, E.-j., Xiang, H.-p., Hao, X.-f., Liu, X.-j., Meng, J.: Crystal structures and elastic properties of superhard Ir_2 and Ir_3 from first principles. *Physical Review B* **76**(5), 054115 (2007)
 - [34] Haines, J., Léger, J., Bocquillon, G.: *Annu rev mater res. Annu Rev Mater Res* **31**(1), 1–23 (2001)
 - [35] Waller, I.: Dynamical theory of crystal lattices by m. born and k. huang. *Acta Crystallographica* **9**(10), 837–838 (1956)
 - [36] Pugh, S.: Xcii. relations between the elastic moduli and the plastic properties of polycrystalline pure metals. *The London, Edinburgh, and Dublin Philosophical Magazine and Journal of Science* **45**(367), 823–843 (1954)
 - [37] Nguyen-Manh, D., Mrovec, M., Fitzgerald, S.P.: Dislocation driven problems in atomistic modelling of materials. *Materials transactions*, 0808040508–0808040508 (2008)
 - [38] Chen, X.-Q., Niu, H., Franchini, C., Li, D., Li, Y.: Hardness of t-carbon: Density functional theory calculations. *Physical Review B* **84**(12), 121405 (2011)
 - [39] Oliver, W.C., Pharr, G.M.: Measurement of hardness and elastic modulus by instrumented indentation: Advances in understanding and refinements to methodology. *Journal of materials research* **19**(1), 3–20 (2004)
 - [40] Birch, F.: Finite elastic strain of cubic crystals. *Physical review* **71**(11), 809 (1947)
 - [41] Zunger, S., Wei, L.: Ferreira, and je bernard. *Phys. Rev. Lett* **65**, 353 (1990)
 - [42] Li, X.-G., Chen, C., Zheng, H., Zuo, Y., Ong, S.P.: Complex strengthening mechanisms in the nbmotaw multi-principal element alloy. *npj Computational Materials* **6**(1), 1–10 (2020)
 - [43] Zong, Z., Lou, J., Adewoye, O., Elmustafa, A., Hammad, F., Soboyejo, W.: Indentation size effects in the nano-and micro-hardness of fcc single crystal metals. *Materials Science and Engineering: A* **434**(1-2), 178–187 (2006)
 - [44] Li, X.: First-principles study of the third-order elastic constants and related anharmonic properties in refractory high-entropy alloys. *Acta Materialia* **142**, 29–36 (2018)

- [45] Lamsal, H., Franson, J., Pittman, T.: Transmission characteristics of optical nanofibers in metastable xenon. *Applied optics* **58**(24), 6470–6473 (2019)
- [46] Lamsal, H.P., Franson, J.D., Pittman, T.B.: Optical pumping in xenon atoms. In: *Frontiers in Optics / Laser Science*, pp. 8–7. Optical Society of America, ??? (2020). <https://doi.org/10.1364/FIO.2020.FTu8C.7>. <http://www.osapublishing.org/abstract.cfm?URI=FiO-2020-FTu8C.7>
- [47] Lamsal, H., Franson, J., Pittman, T.: Maximizing optical production of metastable xenon. *Optics Express* **28**(16), 24079–24087 (2020)
- [48] An, K., Fu, S.: High entropy alloys: Advanced synchrotron x-ray and neutron scattering studies (2020)
- [49] Mishra, A., Priyadarshan, G., Clark, D., Lu, Y., Shi, R.: Theoretical investigations on structural stability and elastic properties of monbtaw-x (=ti/v) high entropy alloys. *Journal of Materials Science Research and Reviews* **4**(1-2) (2019)
- [50] Bhandari, U., Zhang, C., Guo, S., Yang, S.: First-principles study on the mechanical and thermodynamic properties of monbtatiw. *International Journal of Minerals, Metallurgy and Materials* **27**(10), 1398–1404 (2020)